# Role of turbulence for mixing and soot oxidation for an equivalent diesel gas jet during wall interaction studied with LES.

Jan Eismark[1,2], Martin Hammas [1],
Anders Karlsson[1,2], Ingemar Denbratt[2] , Lars Davidson[2]

[1] Volvo GTT, Advanced Technology & Research, [2] Chalmers University of Technology

E-mail: jan.eismark@volvo.com
Telephone: +(46) 31 322 5319
Fax: +(46) 31 661228

**Abstract.** Using applied Large Eddy Simulations (LES), turbulent properties were studied of an equivalent diesel fuel gas jet having a vapour phase penetration equal to a diesel spray. Half of the jet was forced to sharply change direction by impinging upon a curved cylindrical wall. The other half of the jet developed freely along a parallel wall acting as a reference flame. It was shown how turbulent structures of various scales develop along the jet and after wall impingement. The turbulent eddies contribute strongly to air entrainment deep into the jet resulting in an increasing rate of dilution of the jet core downstream of the fuel nozzle.

Calculations of the instantaneous fuel concentration were used to study the total surface area and the kinetic energy of the wrinkled stoichiometric zones itself. The resolved sub-grid scale kinetic energy of the stoichiometric surface was found to be significantly higher on the wall side. Statistics of turbulent quantities were computed across interesting sections showing relations between velocity gradients, turbulent velocity field and the production of turbulence.

The findings were used for a discussion about the role of turbulence for soot oxidation in a real diesel flame. Previous observations in a high temperature, high pressure combustion chamber experiment where turbulent eddies sweep fresh gas into the free jet core were confirmed by the simulations. As observed in the experiments, the LES results indicate that also non-fresh gases, especially on the wall side, may be swept into the jet side. As a result, soot oxidation rate can either increase if oxidant radicals are supplied by the turbulent flow or decrease if the in-rushing gases mainly consist of inert combustion products.

## 1. Introduction

This work addresses diffusion controlled direct injection compression ignition combustion with short ignition delay. For this type of combustion, the liquid phase penetration of the diesel spray is stabilised at typically 10-20 mm for heavy-duty size engine spray while the vapour phase penetration continues to develop. Detailed calibration data are available in literature mainly for sprays developing in a free gas [19, 16, 22, 23]. It has been shown that the vapour phase penetration of a free jet is similar for a non-reacting and a reacting jet where the reacting jet produces somewhat higher penetration values [22].

In a real engine, the combusting vapour phase will interact with the piston bowl wall [1, 9, 11, 21]. The effects of wall interactions are therefore of special interest for the design of a combustion system. In a Diesel engine designed for a low swirl ratio, it can be shown by optical combustion diagnostics that the flames will interact with the piston bowl wall, with each other and with the cylinder head [9]. This sequence of events starts with flame impingement on the wall resulting in a wall jet travelling along the bowl wall which later interacts with both adjacent flames and the cylinder head. As a result of the flame interactions, the main flow of each flame is forced to travel towards the center of the bowl. This flow effect creates one strong vortex on each side of the geometrical spray axis. These vortices, created by the kinetic energy in the fuel sprays and the design of the combustion system, are here referred to as the flame recirculation event.

For this kind of combustion, it is well known that the measured engine-out soot emission level is the net result of two main processes during the combustion: soot formation and soot oxidation. Both processes are of the same order of magnitude so that the net soot emissions become very sensitive for changes of parameters related to these two main processes.

Air entrainment takes place partly in the spray core in the lift-off region close to the fuel injector nozzle and partly in the reaction and oxidation layers at the surface of the wrinkled turbulent flame, hereby referred to as surface air entrainment. The spray-internal entrainment is important for the dilution of the spray internal rich fuel mixture and hence influences strongly on the rate of soot formation [7, 18]. The flame surface air entrainment is responsible for the fuel combustion and soot oxidation rate.

Since wall effects occur far away from the fuel atomisation processes near the nozzle, studies of flame surface air entrainment can be carried out by examining the vapour phase behaviour without taking into account near nozzle fuel atomisation and evaporation processes. This approach has been used in literature to experimentally study air entrainment in a turbulent fuel gas jet [6] and for analysis of enhanced mixing after end of injection (EOI), in this case using large eddy simulations (LES) of an air jet [13].

The combustion takes place in a narrow reaction zone at locally stoichiometric conditions [2]. Analysis of the development of the stoichiometric zone before and during wall interaction is therefore of special interest. Additionally, the formation and oxidation of soot are coupled to the local equivalence ratio Φ [3]. The development of Φ in the studied jet can thus be used as an indicator for likely areas for soot formation and oxidation.

Soot oxidation rate depends on mixing rate, temperature and availability of oxidants like OH and oxygen radicals. The mixing rate is controlled by the air entrainment from surrounding gas into the stoichiometric zones on the flame surface. Soot oxidation during a typical low swirl diesel combustion was in [9] divided into three phases: high temperature soot oxidation during the injection period, spray dilution soot oxidation right after end of injection and late rich zone soot oxidation. The two soot oxidation phases after end of injection (EOI) are related to the mixing created by the flame recirculation event because these vortices remain active after EOI until they dissipate. It was concluded in this study that effective late soot oxidation can result in very low engine-out soot emissions. RANS simulations showed that soot oxidation continues farther downstream after wall interaction than does the soot formation.

In order to further investigate flame to wall effects, an additional study was carried out using a high temperature/high pressure combustion chamber set-up [10]. A reacting single combusting diesel spray impinged on a curved wall with half of the flame. The other half of the flame developed freely along a wall, see fig 1.


**Fig. 1** **<u>Left:</u> Experimental results in a high pressure/high temperature combustion chamber showing a dif fraction type of image where the leading edges of vapour phase and soot can be observed. <u>Right</u>: illustration of hypothesis about interaction between turbulent eddies and transport of OH back into flame surface [10]**

The set-up was analysed using optical methods and RANS simulations. Along the curved wall, OH-radicals were detected in the same regions where soot was detected but also further downstream. It was observed in experimental data that the soot leading edge could sometimes move both faster or slower than the main flow. One interpretation was that the local availability of oxidants could be a limiting factor for the rate of soot oxidation if turbulent eddies transport exhaust products instead of fresh air to the soot leading edge.

A hypothesis was formulated that the turbulent structures may contribute to enhance the soot oxidation rate by transporting reactive oxidants to the combustion zone, see figure 1. On the other hand, the eddies may transport already burnt gas containing a low concentration of oxidants into the mixing zone which slows down the soot oxidation rate. If so, the soot leading edge speed might temporary be lowered until new fresh gas is delivered by a new local vortex. Such effects should be of special importance to understand in order to maintain rich zone soot oxidation late in the cycle.

In order to further analyse these experimental and RANS simulation results, flow simulations with applied large eddy simulations (LES) have been carried out. Along with improved computer capacity, the use of LES has increased to simulate transient Diesel sprays and combustion [2, 12-15, 26, 27]. It has been shown that the flow field to a high degree can be resolved. Various methods have been evaluated to model the sub-grid scale (SGS) turbulent kinetic energy based on zero-dimensional or 1-equation models. The importance has been pointed out to use a fine grid resolution in the jet region and near walls together with appropriate spray inlet conditions [5].

This paper discusses this engineering LES flow simulation set-up, the results and a discussion about how the observations can be coupled to soot oxidation processes in a low swirl diesel engine.

## 2. Objectives

The main objective in this work is to use the capability of LES to resolve turbulent structures to examine in more detail the results in the previous experimental and RANS study [10].

## 3. Research approach

This work was focused on studying the role of turbulence for air entrainment into the flame surface after wall impingement. The approach was to isolate the mixing processes. This was done by reducing the problem to a study of a non-reacting *equivalent gas jet* having equal fuel gas phase penetration to the vapour phase of a diesel spray. The equivalent jet was first validated against experimental data for a free jet in the literature. Thereafter, a curved wall was added to the LES simulation mesh.

Selected parameters to analyse were: velocity field, total stoichiometric jet surface area, iso-curves for equivalence ratio, development of resolved scale kinetic energy, sub-grid scale (SGS) turbulent kinetic energy and the turbulence production term in the transport equation for turbulent kinetic energy.

The work is based on evaluation of the first simulation followed by sensitivity analysis of the gas jet inlet conditions using two further simulations with modified gas jet inlet conditions, see details in section 4.

It is understood that this approach cannot address more than flow and mixing issues related to a real diesel diffusion combustion process. Even so, we think the approach is motivated by arguments given in the introduction and the fact that spray induced turbulence is well known to be necessary to achieve a fast enough mixing for highly transient diffusion controlled combustion in engines. The results are used in a discussion about how turbulent mixing influences soot oxidation.

## 4. LES set-up

The simulations were carried out using OpenFOAM-1.7.1. The compressible combustion solver reactingFoam was modified to be able to handle LES calculations. No chemistry was considered.

Sub-grid scale turbulent kinetic energy was modelled using a zero-dimensional Smagorinsky model.

The table below shows the applied LES set-up.

**Tab. 1 LES Set-up**

| Parameter | Value | Unit | Comments | | Parameter | Value | Unit | Comments |
|---|---|---|---|---|---|---|---|---|
| | | | | | | | | |
| Model fuel | - | - | $C_{16}H_{34}$ | | Initial gas temp. in the chamber | 1000 | K | |
| Nozzle diameter | 0.25 | mm | Square shaped | | Initial pressure in the chamber | 168 | bar | |
| Inlet fuel massflow | 14.1 | g/s | Gas phase | | Chamber air composition, $O_2$ / $N_2$ | 0.23 / 0.77 | | |
| Inlet fuel gas temp. | 447 | K | | | Inlet fuel gas kinetic energy | 9331 | $m^2/s^2$ | $k_{in} = 0.2U_{in}^2$ |
| Inlet fuel gas constant R | 36.79 | $J/kg \cdot K^{-1}$ | | | Initial turbulent kinetic energy in the chamber, k | 0.1 | $m^2/s^2$ | |
| Inlet fuel gas density | 1021.6 | $kg/m^3$ | | | Computational mesh | 6.2M | - | Number of hexahedra cells |
| Inlet fuel velocity, $U_{in}$ | 216 | m/s | | | | | | |

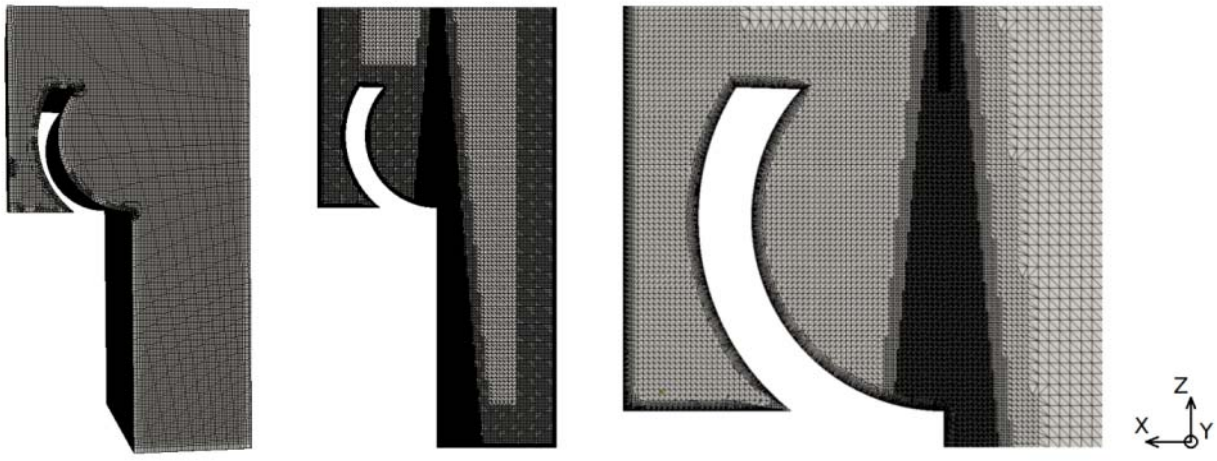


**Fig. 2** Computational mesh

The pictures in Fig. 2 show from left to right the computational domain seen from the side, the refinements and cell distribution in the xz-symmetry plane and the refinements including the eight boundary layers at the curved wall. The first boundary layer thickness is 0.06 mm, then increasing with a ratio of 1.2. The squared inlet consists of $16^2$ cells in the xy-plane, giving a spatial resolution of 0.015625 mm in the cross-section and 0.0625 mm in the streamwise direction of the jet.

The cone-refinement has a resolution of $\Delta x = \Delta y = \Delta z = 0.125$ mm. The centre-region of the curved wall has a cell-size of $\Delta x = \Delta y = \Delta z = 0.5$ mm. The height of the domain is 110 mm. The curved

wall is positioned 50 mm downstream the inlet. The lower part of the domain is 30 mm wide and the upper is twice that size, 60 mm. The gas jet inlet is located at x=y=z=0.

The following numerical schemes have been used for the different terms in Navier-Stokes, continuity equation and the energy equation

**Tab. 2 Numerical scheme**

| Numerical scheme | Terms | Variable fields | Setup |
|---|---|---|---|
| ddtSchemes | $\frac{\partial \phi}{\partial t}$ | All | Backward |
| gradSchemes | $\frac{\partial \phi}{\partial x_i}$ | Pressure | Gauss linear |
| divSchemes | $\frac{\partial (\phi \cdot u_i)}{\partial x_i}$ | Velocity | Gauss limitedLinearV 1 |
| divSchemes | $\frac{\partial (\phi \cdot u_i)}{\partial x_i}$ | Fuel concentration Enthalpy | Upwind |
| laplacianSchemes | $\mu \frac{\partial^2 \phi}{\partial x_i^2}$ | All | Gauss linear corrected |

In order to obtain a numerically stable solution, the Courant number (CFL) should be below unity. A timestep of $10^{-8}$ was used in the simulations. The CFL is defined as

$$CFL = \Delta t \sum_{i=1}^{n} \frac{u_i}{\Delta x_i} \text{ , n=3}$$

The inlet flow initial conditions were in the first simulation uniform. In the two following simulations, randomized turbulent inlet conditions were generated using the algorithm:

$$U_{turb} = U_{ref} + I \cdot U_{ref} \cdot r$$

where I = turbulent intensity and r = random number $-1 \le r \le 1$ .

The applied near wall grid resolution was acceptable according to calculated Wall units , which were well below unity.

## 5. Validation

The gas jet was injected with an assumed density whereafter the boundary conditions nozzle gas jet velocity and nozzle hole area were calibrated such that the gas phase penetration corresponded to vapour penetration data for a free diesel spray [19] while the control volume pressure and temperature matched these experimental conditions. The results in Fig.3 show an acceptable agreement between simulation and experiments.

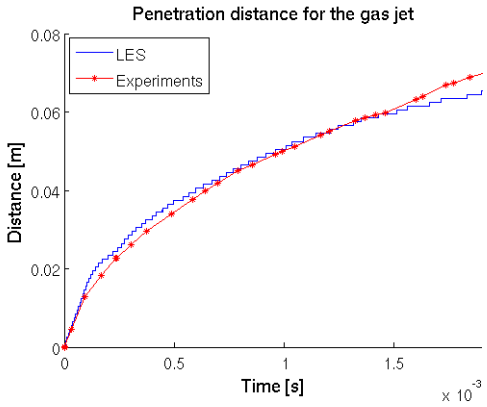


**Fig. 3** **Validation of equivalent gas jet model. Comparison of gas jet penetration distance for a free jet. Solid line: experimental results [19]. Dotted line: LES uniform inlet results.**

## 6. Results

This section contains a presentation and analysis of the results. First, the main features of the flow field are illustrated. Next steps are to evaluate the stoichiometric surface of the jet and the air entrainment followed by studies of iso-contours of equivalence ratios of interest. Finally, resolved kinetic energy, sub-grid scale turbulent kinetic energy and production of turbulent kinetic energy are studied.

### *6.1 Definition of studied cross-sections and sampling locations*

In the following plots, cross-sections shown in Fig. 4 were selected. Also shown are the positions for sampling of data, see section 6.6.

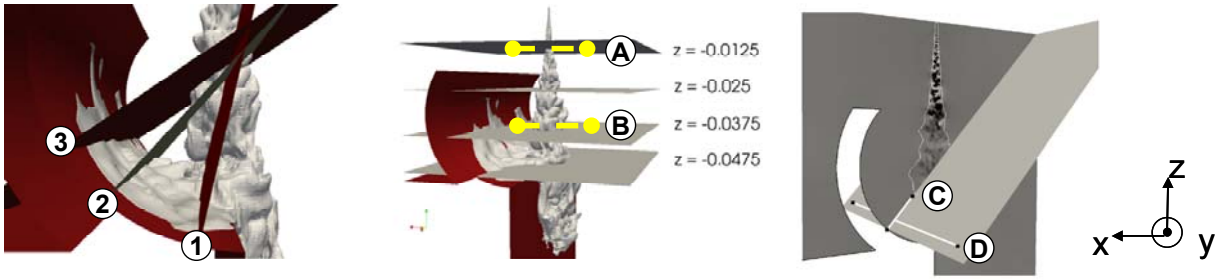


**Fig. 4** **Location of cross sections in following figures. A-D=positions of virtual probes A: z= -12.5 mm, y = 0, x=sampling line, B: z= -37.5 mm, y = 0, x=sampling line, C: wall normal at plane 2, y = 0, angle 41°.D: y=sampling line at 3 mm normal distance from wall, x and z=constant.**

### *6.2 Main features of the flow field*

Fig. 5 shows the instant fuel concentration for the three LES simulations in a cross-section along the center of the jet just before wall impingement (t=1.2 ms). The jet tip penetration, global dimensions and size of turbulent structures on the side of the jets are similar. The local fuel concentration is as expected for a turbulent flow different except at the jet tip where the turbulence is low. The basically similar results with three different inlet gas jet profiles show that the simulation results are sufficiently robust regarding the inlet conditions.

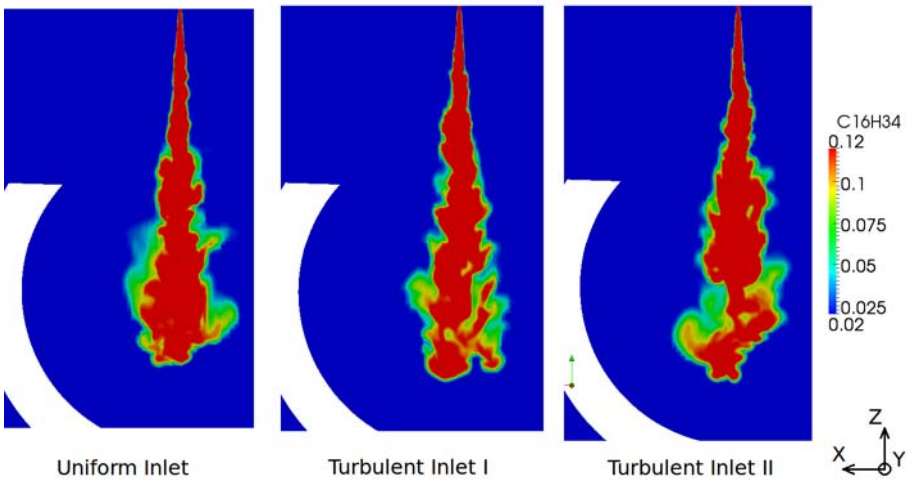


**Fig. 5** **Comparison of the three LES-simulations at 1.2 ms. The plots show fuel concentration.**

### *6.3 Stoichiometric surface*

An overall view of the mixing is given by studying the stoichiometric surface which was calculated by interpolation of the fuel concentration field at stoichiometric mixture. The stoichiometric surface area was calculated as:

$$property(isosurface) = \int_0^t \int_{-x}^{0} f(x,t)dxdt + \int_0^t \int_0^x f(x,t)dxdt$$

where f(x,t) is the field having stoichiometric mixture

The first term corresponds to the curved side of the jet and the second term is the free side.

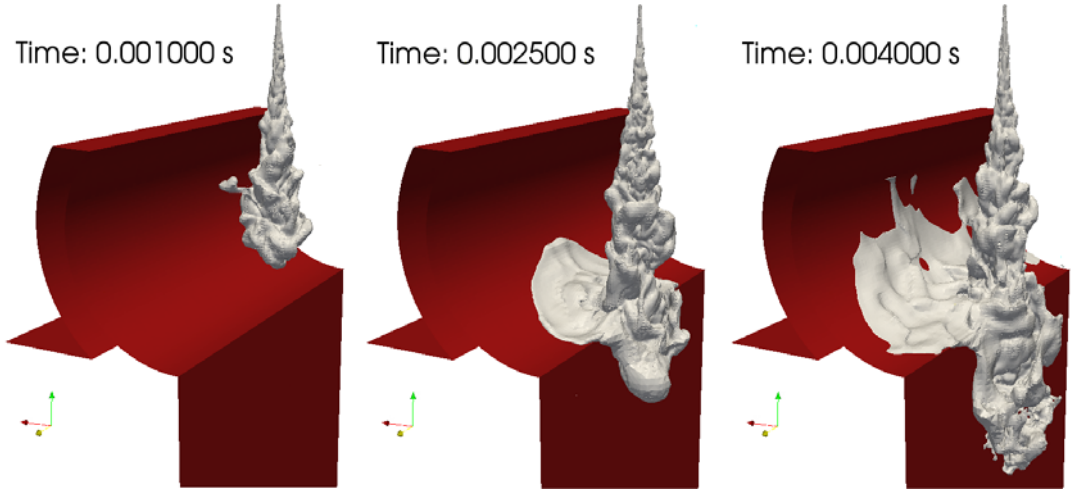


**Fig. 6** **Instantaneous stoichiometric surface development.**

It can be seen in Fig. 6 that the jet on the curved wall side develops wall jet structures in a rather thin layer along the surface. On the reference side of the jet, turbulent structures continue to develop after the jet impingement . The structures on the two sides are obviously different.

### *6.4 Air entrainment*

The flow situation in horizontal cross sections were taken at three vertical distances on the free part of the jet and upon wall impingement, see Fig. 7. The velocity field is here colored corresponding to the fuel concentration. In Fig. 8, planes 1,2 and 3, which are situated in the normal direction at three positions along the curved wall, are presented with the same type of plots.

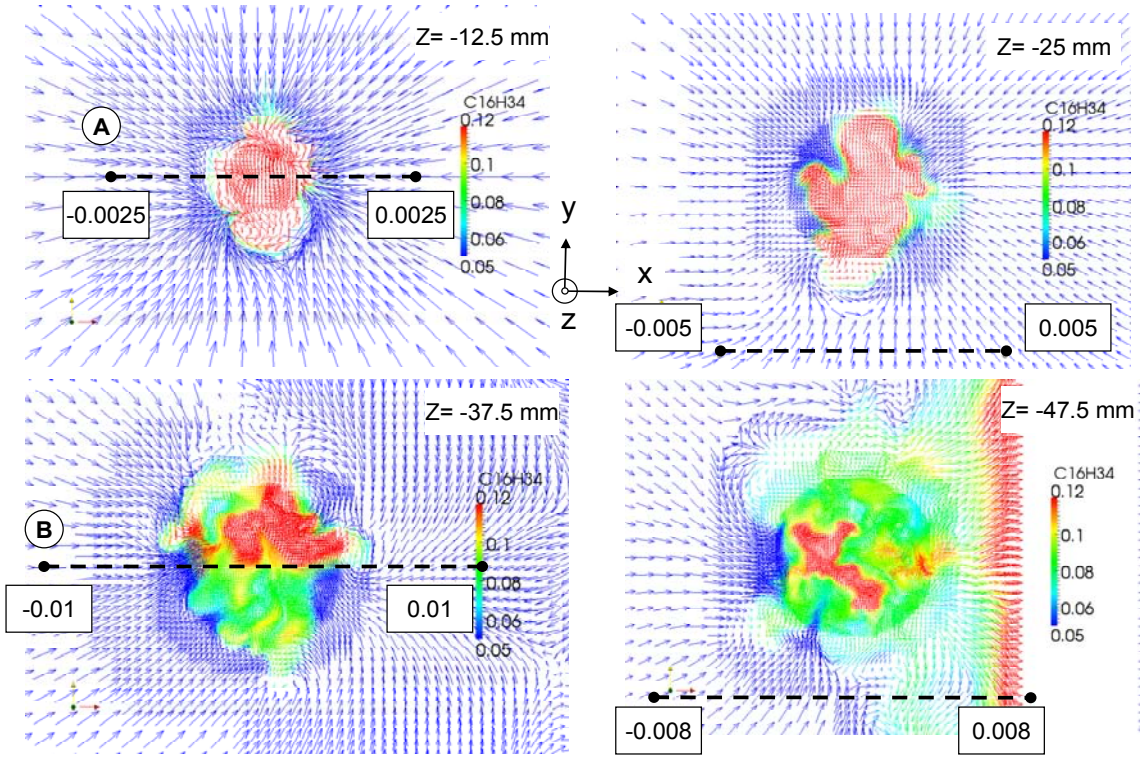


**Fig. 7** **Horizontal velocity field and mixing seen from below at four z-levels taken at 4 ms injection duration. Positions for the sampling lines A and B are found in the two left figures. The lower right cross section is situated in the impingement zone.**

The above figures illustrate the nature of radial flow patterns towards the rich center of the free jet. It can be see how LES resolves several small turbulent structures in the jet. The turbulent structures contribute to enhanced mixing along the jet axis which is seen by the increasing dilution especially when pairs of counter-rotating vortices forces fresh gases to travel into the jet.

A corresponding observation is found in a vertical cross-section, see Fig. 8

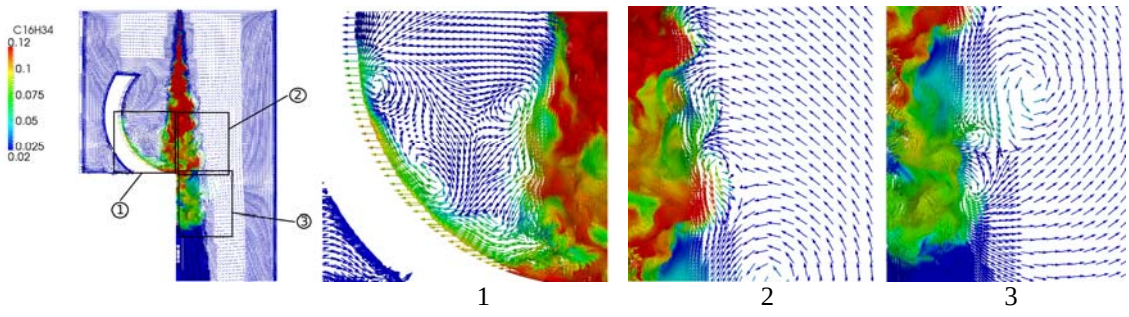


**Fig. 8** **Instantaneous xz velocity field at 3 ms after start of injection colored by fuel concentration. Left: curved wall side, middle: free jet side, right: jet tip**

The turbulent structures occur downstream of the nozzle exit and start to develop to larger and larger vortices along the jet side. This is as expected since the large velocity gradients between the high velocities in the streamwise jet direction (-z) and the surrounding quisent gas create vorticity kernels that receive kinetic energy from the main jet flow. The turbulent flow structures entrain air into the jet core with increasing intensity along the jet axis.

After wall impingement, the jet starts to develop wall jet structures found as several small vortices, see Fig. 9. The pulsating turbulent flow from the free main jet is transformed to a sequence of wall eddies along the curved wall. They are able to entrain fresh air into the wall jet structure.

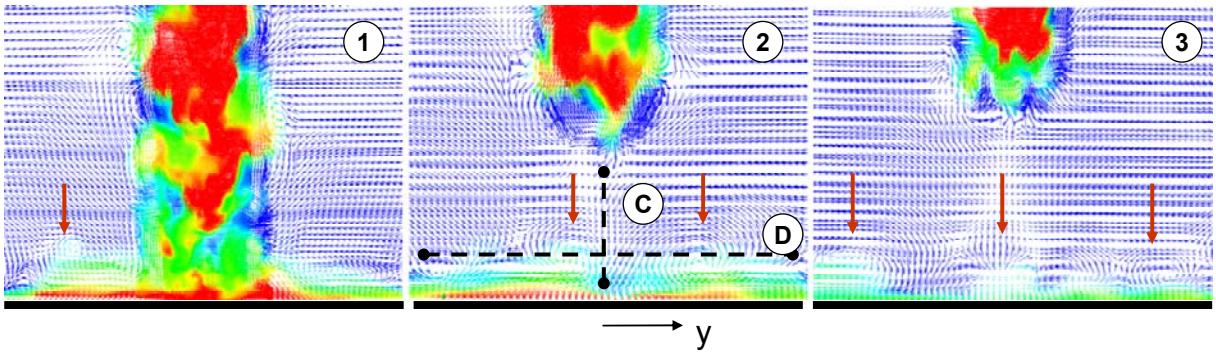


**Fig. 9** **Velocity field and mixing at three planes perpendicular to the curved wall (angles 10 °,25 ° & 41 ° ) at 4 ms after start of injection, see Fig 4. Position for the sampling lines C and D are found in the middle picture. Wall vortex structures are indicated with red arrows.**

The jet tip is pushing gas in front of its leading edge which creates an increase in pressure near the wall. The created wall jet is rather thin due to the pressure field.

### *6.5 Equivalence ratio iso-contours*

Four levels of equivalence ratio (**Φ)** iso-curves were used to further study the development of the mixing based on important combustion parameters: rich zones where soot can be formed, stochiometric zone where combustion takes places, slightly lean conditions where soot oxidation preferentially occurs and vapour phase penetration, see table below.

**Tab. 3** **Identification of equivalence ratio iso-curves**

| **Fuel (%mass)** | **Equivalence ratio Φ** | **Remark** |
|---|---|---|
| 12 | 2 | **Φ** =2 : soot formation range (black diamonds) |
| 6 | 1 | **Φ** =1: stoichiometric combustion zone (red circles) |
| 5 | 0.83 | **Φ** <1: slightly lean soot oxidation range (green stars) |
| 0.1 | 0.02 | **Φ** <<1: vapour phase penetration (blue +) |

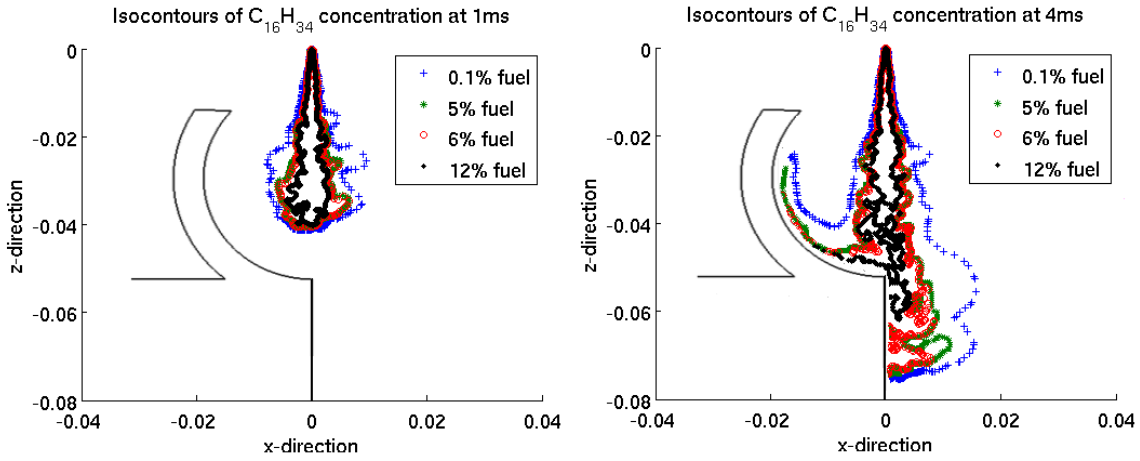


**Fig. 10** **Iso-equivalence ratio curves in x-z plane, y=0 (jet center). Black filled diamond :Φ=2, Red circle: Φ=1, Green star: Φ =0.83, Blue + : Φ =0.02.**

As presented in Fig. 10, the likely zone for soot formation processes, inside the **Φ** = 2 iso-surface, is large and fluctuating. Between this zone and the stoichiometric area a certain distance appears. Formed soot is likely to be transported over this intermediate zone rather than to continue to form soot since the equivalence ratio here is smaller than 2. Nor can the soot be oxidized since the mixture still is rich.

The **Φ** = 1.0 and **Φ** = 0.83 iso-curves are found near each other forming a thin wrinkled layer with favourable conditions for both combustion near **Φ** =1.0 and soot oxidation on the lean side. The **Φ** = 0.02 vapour leading edge iso-curve corresponds fairly well with the experimental observations on the same set-up [10]. The wrinkling (in experiments and simulations) is much more pronounced near and just below **Φ** =1.0 than for the vapour leading edge contour **Φ** =0.02.

### *6.6 Resolved kinetic energy and SGS turbulent kinetic energy*

In order to study how the injected kinetic energy is distributed, the resolved kinetic energy K and subgrid scale modelled turbulent kinetic energy $k_{sgs}$ were calculated for the entire field as:

Resolved kinetic energy $K = \sum(\rho U_i U_i)$ ( $kg/ms^2$ )

The quantity $k_{SGS}$ was calculated from the implemented Smagorinsky model as:

$$k_{sgs} = \left( \frac{\nu_{SGS}}{\Delta \cdot C_s} \right)^2$$

where

$C_s$ is the Smagorinsky model constant

$\Delta$ is the local cell size

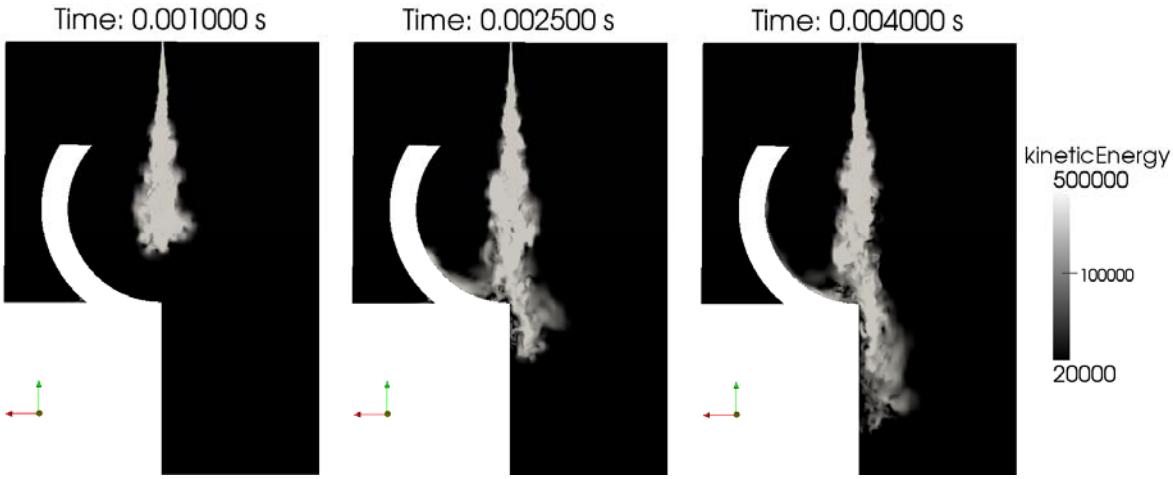


**Fig. 11** **Resolved kinetic energy K (kg/ms$^2$) in the xz-plane at 1, 2.5 and 4 ms.**

The resolved kinetic energy shown in Fig. 11 is as expected highest near the jet core where the velocity is highest. Since new kinetic energy in this set-up is continuously supplied through the nozzle flow, the kinetic energy field covers an increasing volume. K is comparably weak along the curved wall side.

The small scale SGS turbulent kinetic energy is of interest to study since the combustion reactions in the this stoichiometric layer are assumed to take place on this scale [2].

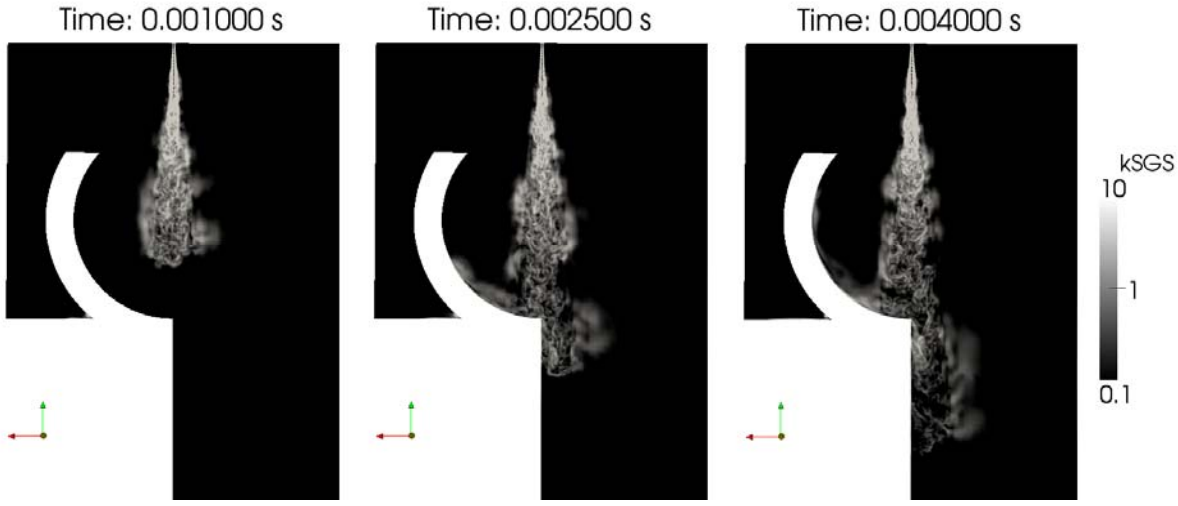


**Fig. 12** **Sub-grid scale turbulent kinetic energy $k_{sgs}$ (m$^2$/s$^2$) in the xz-plane at three occasions**

.

Observations on $k_{sgs\ in}$ Fig. 12 are that its magnitude is just a fraction of K in magnitude, it shows a wider distribution than for K and the field is more diluted.

Finally, the two kinetic energies of the stoichiometric iso-surface were computed.

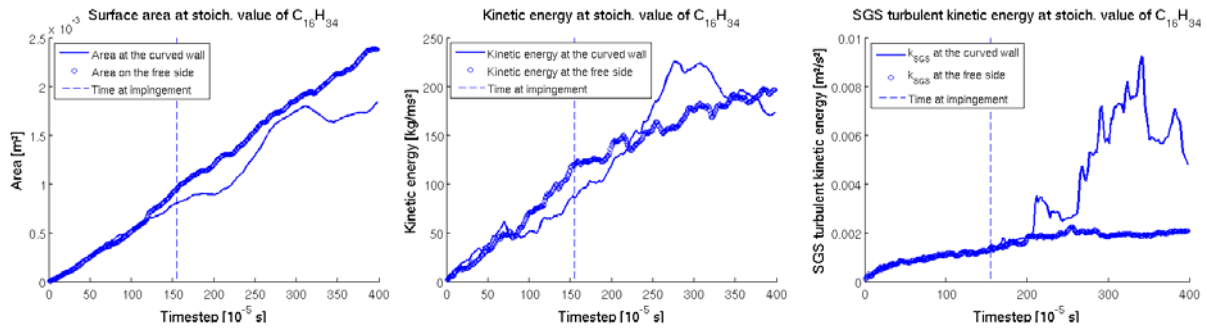


**Fig. 13** **Comparisons of free side (dotted) and curved side (thin solid line). Left: Stoichiometric surface area, middle: resolved turbulent kinetic energy k of stoichiometric cells, right: modelled turbulent kinetic energy $k_{sgs}$ of stoichiometric cells . Dashed vertical line is the start of jet impingement.**

In Fig. 13 it can be seen in the left plot that the instantaneous stoichiometric surface on the wall side, upon wall impingement at 1.5 ms is lower than on the free side. Middle plot shows that there is a decay in K on the curved wall side but at 2.5 ms, K becomes larger on the curved side than on the free side, in spite of the lower surface area. This is consistent with the observation that wall vortices need some time to develop. The higher level lasts until 3 ms when it becomes lower once again.

The effect of the wall impingement on $k_{sgs}$ is very pronounced, see right plot in Fig. 13. The $k_{sgs}$ is in fact clearly higher on the curved wall side after wall impingement than on the free side. The interpretation is that small scale turbulence increases by the increase of the strain rate and the small cell size ( $\Delta$ ) in the Smagorinsky model. $k_{sgs}$ also decays by the end of the simulation period. A possible explanation for the decay is that the availability of lean gases becomes lower due to the limited space between the side of the free jet and the wall jet. As a result the stoichiometric surface area will be lowered by turbulence driven supply of rich gases which also somewhat lowers the turbulent kinetic energy in the stoichiometric cells.

### *6.7 Production of turbulent kinetic energy analysed using "Virtual probe" data*

Bearing in mind that the LES set-up uses the most simple sub-grid scale model (zero-dimensional), an examination of the flow was carried out along four "virtual sampling probes" defined in Fig. 4 . The objective was to study the production term in the transport equation for turbulent kinetic energy. The production term is as follows:

$$P^k = -\overline{u_i' u_j'} \frac{\partial \overline{u_i}}{\partial x_j}$$

where $u_i' = u_i - \bar{u}_i$ and $\frac{\partial \overline{u_i}}{\partial x_j}$ = the spatial gradient field of the mean velocity.

The parameters: instant velocities and spatial gradients were extracted at 150 equidistant points in space along each sampling line with a sampling step of 0.01 ms. The fluctuating velocities were calculated using the average values of the instantaneous velocities. The first value was taken when the flow had reached turbulent conditions on the basis of time series which was possible for the probes located in the free jet.

It was found that the flow on the wall side did not show truly turbulent behaviour since, for instance, no stable mean values were reached. Instead, complex eddy patterns were detected with a large timescale originating from the wall vortex structures passing by the sampling line, see Fig. 14. As a consequence, the production term was only calculated for the free jet at sampling lines A and B.

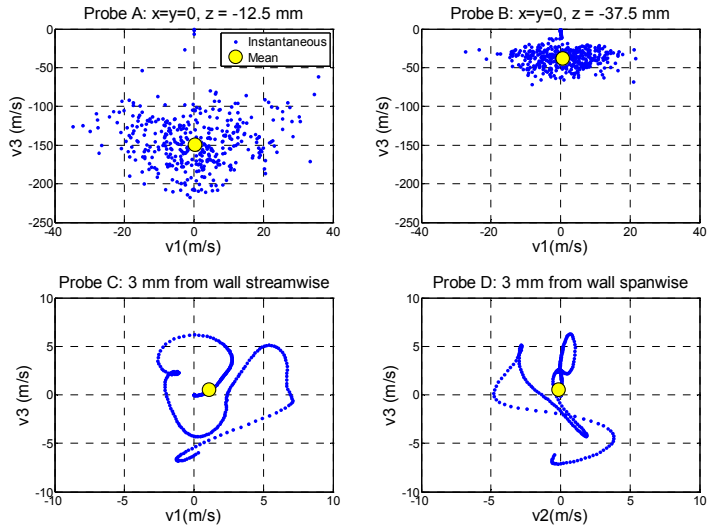


**Fig. 14** **Scatter plots of velocity vector paths during the gas jet injection period at the four sampling lines A-D.**

As indicated in the lower two plots in fig 14, a sequence of clearly three-dimensional and complicated patterns occurred at both the wall-normal and spanwise sampling lines on the curved wall side.

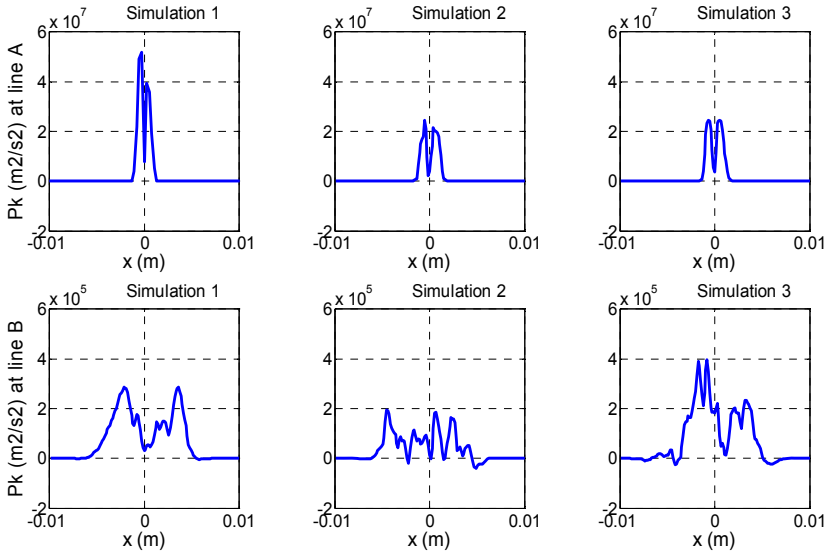


**Fig. 15** **Pk calculated at probe A and B. Data were extracted from simulation 1,2 and 3 respectively.**

The production term is found in Fig. 15. At the nozzle-near sampling line A, the axial-radial element of Pk dominates due to the strong axial-radial velocity gradient. Turbulent kinetic energy is thus mainly produced in the shear layers between the jet and the quisent air. Further downstream, at sampling line B, Pk has reduced to approximately 1/100 in magnitude. The production occurs over a wider distance since the jet has now been more diluted by the produced turbulent structures upstream in the jet.

A final remark is that the first simulation with uniform inlet velocity profile (simulation 1) resulted in higher turbulence production near the nozzle than with randomized turbulent inlet profiles (simulation 2). It can also be seen at sampling line B that the dilution is more elevated with randomized turbulent inlet profiles.

## 7. Discussion

The applied LES set-up provided interesting results. However, there are several issues to take into account in the analysis. The low number of LES-simulation (three) is not possible to use for statistical analysis of the entire flow field since several hundred simulations would be needed. That number of LES-simulation is out of reach due to the time-consuming computation. The main reason for this is the high number of computational cells. The computation time is proportional to number of grid cells to the power of three. Another issue is that the selected zero-dimensional subgrid scale model is a limitation for how well the small scale turbulence is treated.

The simulation results of the resolved field correspond qualitatively well with literature regarding the appearance and main features of the turbulent flow field. For instance, in the experimental results with the same geometry as analysed with LES in this paper, the appearance of the flow on the wall side is similar regarding the thickness of the jet and the behaviour of the wall jet eddies. Another important similarity is the observation that zones can be de-coupled from the main wall jet flow.

The air entrainment results correspond well with the extensive experimental results in [6]. The research team used particule image velocimetry (PIV) analysis of a free jet as well as of an impinging jet. This work illustrates how turbulent structures evolve along the jet, transporting fresh gases deep into the jet. The quality of the measured flow patterns is very similar to the results from LES in this paper.

Complicated vortex structures on the curved wall side were observed. The time-scale of these vortices was considerable larger than for the vortices along the free jet. The wall side flow shows fast changes in velocity magnitude and direction meaning that the strain rate is high. The vortices are therefore considered as energy carrying eddies that provide turbulent kinetic energy to the subgrid scale mixing. Consequently, the calculations of the SGS turbulent kinetic energy $k_{sgs}$ showed a significantly higher level on the curved wall side than on the reference side.

Under the assumption that oxidation occurs at the small length-scales covered by the subgrid scale, oxidation is also promoted. It should though be noted that the flow could not be analysed regarding its turbulent nature as for the free jet due to the large time-scale. A large number of simulations would be needed to define if the observed eddies can be considered as chaotic (turbulent).

De-coupling of small rich zones from the main flow on the curved wall jet side was observed in the combustion chamber study, in the RANS simulations as well as with LES. LES provides an understanding of how local turbulence is produced and contributes to the de-coupling. Such zones were rapidly diluted (or burned in the combustion chamber experimental set-up) when they were transported into low equivalence ratio areas. On the other hand, the rich zones may be transported into areas with high equivalence ratio if the zones appear near the main free jet. In this situation, the conditions for oxidation are poor and the rich zone can remain late into the cycle.

Applying the observations above to a real engine combustion system, two competing processes can be identified. Firstly, the jet - wall interaction should increase the local mixing rate and hence the soot oxidation rate. Secondly, the limited space between two main jets can lead to a situation when de-coupled zones from the wall jet are transported into zones with combustion products which should decrease the mixing rate. If the de-coupled zones do not reach fresh air with sufficient temperature for oxidation before the turbulence has dissipated, the zones will remain incompletely burned. Such unburned zones contribute to higher engine-out soot emissions.

A final remark is that the instantaneous equivalence ratio field according to the LES results in this work is very different from the general conceptual model of a diesel flame which is based on average values. The observed in-rushes of fresh air through the jet surface into the jet core due to turbulence could even impact on the soot formation rate if the local equivalence ratio becomes sufficiently low ($\Phi<2$).

## 8. Conclusions and future work

The role of turbulence for mixing and creation of favourable conditions for soot oxidation were investigated using LES-simulations of a high speed, dense gas jet with a penetration equivalent to the vapour phase of a diesel spray. The results show how a turbulent transient flow field develops, first as a free jet, and later impinging with a curved wall. Turbulent structures were resolved showing how the stoichiometric surface of the wrinkled jet is interacting with the surrounding gas and with the curved wall. The simulation results were qualitatively similar with previous experimental measurements on the same geometrical set-up and with other similar experiments in literature.

The turbulence creates complex local vortex structures that strongly influence on the local air entrainment along the jet sides and deep into the jet core. The formed turbulent structures in the free jet are after wall impingement transformed to a sequence of complex vortices with a large time-scale. The vortices are suggested to be energy carrying eddies that provide kinetic energy to the sub-grid scale mixing. Due to the low number of simulations, it could not be concluded whether the wall flow eddies can be considered as a turbulent flow.

The results were used for a discussion about the role of turbulence for soot oxidation in a real diesel engine combustion situation. Two competing processes were identified for the impact of wall impingement. The wall vortices contribute to soot oxidation by increased local mixing in the small length scales. On the other hand, late in the cycle when an increasing amount of combustion products become available, the wall vortices may transported inert gases to the soot oxidation zones which should decrease the soot oxidation rate.

In future work, LES with wall functions could be applied. Wall functions for the near wall flow and LES to resolve the outer flow would then be used. This method would lower the computation time significantly since the mesh near the wall can be designed with fewer cells. Additionally, the solution would rely on the accuracy of the wall model instead of a very high mesh resolution in the wall normal direction. This approach should be acceptable if the objective is to study mixing in the free flow rather than near wall effects.

In the event that computation time can be lowered significantly in the future, it would be interesting to perform a large number of simulations to study the impact of the near wall boundary layer on the solution, the turbulent nature of the wall side flow and investigate if the average solution will be similar to the diesel flame conceptual models in literature.

## 9. Acknowledgements

The Swedish Energy Agency (30754-2) and Volvo Corporation are both acknowledged for the joint funding of this work. Thanks to Anders Rynell for contributing to set-up this simulation environment.

## 10. References

1. Aronsson. Processes in Optical Diesel Engines. Doctoral Thesis. Lund University of Technology 2011.
2. Baudoin. Large Eddy Simulation of Turbulent Premixed and Partially Premixed Combustion. Doctorial thesis. Lund University 2010.
3. Balthasar. Detailed soot modelling in laminar and turbulent reacting flows. Doctoral thesis. Lund University 2000.
4. Balthasar, Magnusson and Eismark. Soot modelling in HD diesel engine. Combustion generated fine carbonaceous particle. Proceedings of an International Workshop held in Villa Orlandi, Anacapri, may 13-16, 2007.
5. Banarjee and Rutland. On LES Grid Criteria for Spray Induced Turbulence. SAE-paper 2012-01-0141
6. Bruneaux, Causse and Omrane. Air entrainment in Diesel-like gas jet by simultaneous flow velocity and fuel concentration measurements, comparison of free and wall impinging jet configurations. SAE 2011-01-1228.
7. Chartier. Spray Processes in Optical Diesel Engines. Doctorial thesis. Lund University 2010.

8. Davidson Lars. Textbooks on turbulent theory. Chalmers University of Technology. http://www.tfd.chalmers.se/~lada/postscript_files/solids-and-fluids_turbulent-flow_turbulence-modelling.pdf
9. Eismark, Balthasar, Carlson, Benham, Christensen and Denbratt. Role of late soot oxidation for low emission combustion in a diffusion-controlled, high-EGR, heavy duty diesel engine . SAE-paper 2009-01-2813, 2009
10. Eismark, Karlsson, Lindgren, Magnusson, Ochoterena and Denbratt. Role of formation and transportation of hydroxyl radicals for enhanced late soot oxidation in a low emissions heavy-duty diesel engine**.** Thiesel 2010 proceedings.
11. Genzale, Reitz and Musculus. Effects of Piston Bowl Geometry on Mixture Development and Late-Injection Low-Temperature Combustion in a Heavy-Duty Diesel Engine. SAE-paper 2008-01-1330.
12. Hori, Senda, Kuge and Fujimoto. Large Eddy Simulation of Non-Evaporative and Evaporative Diesel Spray in Constant Volume Vessel by Use of KIVALES. SAE-paper 2006-01-3334.
13. Hu, Musculus and Oefelein. Large Eddy Simulation of a Transient Air Jet with emphasis on Entrainment during Decelaration. SAE-paper 2010-01-1133.
14. Kaario, Pokela, Kjäldman, Tiainen and Larmi. LES and RNG Turbulence Modeling in DI Diesel Engines. SAE-paper 2003-01-1069.
15. Lee, Pomraning and Rutland. LES Modeling of Diesel Engines. SAE-paper 2002-01-2779.
16. Magnusson. Spray-Wall Interactions of Diesel Sprays. Doctoral thesis. Chalmers University of Technology 2009
17. Miles, Megerle, Hammer, Nagel, Reitz and Sick. Late-Cycle Turbulence Generation in Swirl-Supported, Direct-Injection Diesel Engines. SAE paper 2002-01-0891.
18. Musculus and Kattke. Entrainment Waves in Diesel Jets. SAE paper 2009-01-1355.
19. Naber and Siebers, Effects of Gas Density and Vaporization on Penetration and Dispersion of Diesel Sprays. SAE-paper 960034.
20. Ochoterena. Optical Diagnostics of Soot in Combusting Sprays. Doctorial thesis. Chalmers University of Technology 2009.
21. Pickett and Lopez 2005 . Jet-Wall Interaction Effects on Diesel combustion and Soot Formation. SAE paper 2005-01-0921
22. Pickett, Genzale, Bruneaux, Malbec, Hermant, Christiansen and Schramm. Comparison of Diesel Spray Combustion in Different High-Temperature, High-Pressure Facilities. SAE-paper 2010-01-2106.
23. Pickett, Manin, Genzale, Siebers, Musculus and Idicheria. Relationship Between Diesel Fuel Spray Vapor Penetration/Dispersion and Local Fuel Mixture Fraction. SAE-paper 2011-01-0686.
24. Pope. Turbulent flows. Cambridge University Press 2000.
25. Rynell and Hammas. A study of turbulence phenomena in simplified flow situations of interest for diesel combustion development. Master Thesis Work. Chalmers University of Technology 2011.
26. Solsjö and Bai. Injection of Fuel at High Pressure Conditions: LES Study. SAE-paper 2011-24-0041.
27. Solsjö, Jangi, Tuner and Bai. Large Eddy Simulation of Partially Premixed Combustion in an Internal Combustion Engine. SAE-paper 2012-01-0139.

**Contact** jan.eismark@volvo.com